Applied Catalysis B: Environmental 176–177 (2015) 464–471

Contents lists available at ScienceDirect

Applied Catalysis B: Environmental

journal homepage: www.elsevier.com/locate/apcatb

Fabrication and photoelectrochemical study of WO_3-based bifunctional electrodes for environmental applications

Sapanbir S. Thind [a], Kyle Rozic [a], Fumiaki Amano [b], Aicheng Chen [a,*]

[a] Department of Chemistry, Lakehead University, 955 Oliver Road, Thunder Bay ON P7B 5E1, Canada
[b] Faculty of Environmental Engineering, The University of Kitakyushu, 1-1 Hibikino, Wakamatsu-ku, Kitakyushu 808-0135, Japan

ARTICLE INFO

Article history:
Received 7 February 2015
Received in revised form 5 April 2015
Accepted 16 April 2015
Available online 17 April 2015

Keywords:
WO_3 nanoplatelets
Hydrothermal method
Pt nanoparticles
Photocatalysis
Visible light activity

ABSTRACT

In this study, unique WO_3-based bifunctional electrodes were prepared with the aim of achieving optimal photocatalytic and electrocatalytic activities of WO_3 nanoplatelets and Pt nanoparticles, respectively. WO_3 nanoplatelets with a high visible light response were directly grown on both sides of a tungsten substrate via a facile hydrothermal method. Pt nanoparticles were deposited on one side of the WO_3 electrode, where they served as the electrocatalyst. The prepared electrodes were characterized by X-ray diffraction (XRD), scanning electron microscopy (SEM), electron dispersive X-ray spectroscopy (EDS) and cyclic voltammetry. Our experimental results revealed that the synthesized WO_3 electrodes possessed high photochemical activity under visible light exposure, whereas the deposition of Pt nanoparticles with a large electrochemical active surface area significantly enhanced the electrocatalytic activity of the electrode. Various sets of photodegradation reactions involving Rhodamine B (RhB) were conducted to evaluate the efficacy of the WO_3 electrodes, prior to and following the deposition of Pt nanoparticles under both visible light and applied potential. The bifunctional electrode exhibited far greater activity as compared to the WO_3 electrode as the sole photocatalyst and WO_3–Pt as the sole electrocatalyst, very promising for energy and environmental applications.

1. Introduction

Over the last few decades, considerable attention has been focused on the development of technologies that may be utilized in the eradication of anthropogenically generated environmental pollution [1]. Traditional wastewater treatment techniques are typically activated through electrosorption, chemical oxidation and biological digestion [2–4]. Heterogeneous photocatalysis is a promising alternative technique for the eradication of organic pollutants in wastewater [5,6]. Heterogeneous photocatalysts function by absorbing incident light, which results in the activation of materials that subsequently initiate a sequence of chemical reactions of interest. Various semiconductors, such as TiO_2, CdS, SnO_2, WO_3, SiO_2, ZrO_2, ZnO, Nb_2O_3, Fe_2O_3, $SrTiO_3$, CeO_2, Sb_2O_4, V_2O_5, C_3N_4 have been widely studied by various research groups recently [7–12]. Among these investigated materials, TiO_2, WO_3 and ZnO have demonstrated very promising results [13–17]. TiO_2 is the most extensively studied of these semiconductor materials due to its stability, non-toxicity, and high inertness. However, it has the drawback of being activated solely by UV light due to its large band gap. Thus TiO_2 requires structural and electronic modifications to facilitate its activation via ambient sunlight [18–20]. Significant efforts have been made by doping TiO_2 with metals, non-metals, or by its being coupled with WO_3 to enable the capacity to absorb visible light [21,22]; one of the most important aspirations of modern science is the achievement of the efficient utilization of solar energy.

Since WO_3 possesses a lower band gap (ca. 2.6–3.0 eV), it may be employed as a visible light-driven photocatalyst because of its unique electronic properties [23–26]. Due to its ability to absorb in the visible light region, along with other properties, WO_3 has been gaining in popularity for its use in photoelectrochromic "smart" windows, solar energy conversion, storage cells, solar water-splitting cells, and as a potential catalyst enhancer for fuel cells, photocatalysis, batteries, and gas/chemical sensors [27–31].

On the other hand, electrocatalysts are widely employed in large electrolytic processes that require significant energy. Currently, electrocatalysts are utilized in industry in order to decrease manufacturing expenditures by reducing the amount of electric power that is required for specific processes. Transition metals dominate in electrocatalysis due to the presence of unpaired d electrons and unfilled d orbitals, which form bonds with adsorbates [32]. The

* Corresponding author. Tel.: +1 807 3438318; fax: +1 807 346 7775
E-mail address: aicheng.chen@lakeheadu.ca (A. Chen).

http://dx.doi.org/10.1016/j.apcatb.2015.04.033
0926-3373/

fundamental advantages of electrochemical oxidation processes include ease of operation, a wide range of possible treatment conditions and environmental compatibility [33]. One of the most efficient electrocatalysts is Pt, which has been intensively investigated for its utility in fuel cells and electrocatalytic applications [34–37]. It has also been reported that platinized WO_3 shows high photocatalytic activity on the degradation of organic pollutants [38,39].

In this study, for the first time, WO_3 based bifunctional electrodes have been fabricated, wherein platelet-like structures comprised of WO_3 were synthesized via a hydrothermal method. The WO_3 electrodes were found to possess a high visible light response. To amalgamate the photocatalytic activity of WO_3 and the electrocatalytic activity of Pt nanoparticles, Pt was deposited on one side of the WO_3 electrodes, resulting in the creation of a bifunctional electrode. The prepared electrodes were examined by utilizing various surface analytical methods. To demonstrate the high catalytic activity of the prepared electrodes, photochemical and photoelectrochemical degradation of Rhodamine B (RhB) was performed under various applied conditions. The bifunctional electrode exhibited much greater activity as compared to the WO_3 electrode as well as the WO_3–Pt electrode.

2. Experimental

2.1. Materials

Tungsten plates, having a thickness of 0.25 mm, were obtained from Sigma–Aldrich (99.9% trace metals basis) and cut into 1 cm × 1 cm squares. Acetone (≥99.5%), nitric acid (70%), and H_2SO_4 (99.999%) were purchased from Sigma–Aldrich and used as received. Rhodamine B (BDH, UK) was employed as a typical model of an organic dye pollutant in the evaluation of the photocatalytic and electrocatalytic activity of the WO_3 based catalysts. Water (18:2 MΩ cm) used in the preparation of the aqueous solutions was purified utilizing a NANOpure® Diamond™ water system.

2.2. Photocatalyst synthesis

To prepare the WO_3 photocatalysts, a facile hydrothermal method was employed, wherein a commercially available tungsten plate (Sigma–Aldrich, 99.7%) was cut to obtain a 1.0 cm^2 area, which was used as a substrate. The tungsten plates were then sonicated multiple times in acetone to remove any surface resident organic impurities, followed by sonication in water. In order to grow tungsten oxide on the substrate, it was introduced into a Teflon lined autoclave, with 60% of its volume filled with 1.5 M HNO_3. The hydrothermal cell was then introduced into a furnace, which was heated to 180 °C for one hour. Following the hydrothermal treatment, the electrodes were rinsed with ultrapure water several times and then heated to 450 °C over three hours and used in electrochemical tests as such, subsequent to calcination.

2.3. Deposition of Pt nanoparticles on the WO_3 electrode surface

WO_3 electrodes containing Pt nanoparticles were fabricated using a photochemical reduction method. In general, a 0.1 mM solution of an inorganic $H_2PtCl_6{\cdot}6H_2O$ precursor was formulated in ultrapure water. A desired amount of this solution was added into 5 mL of a 50% (v/v) methanol solution, which was deaerated for 10 min with ultrapure argon gas to eliminate any oxygen that remained in the solution; the test tube was then sealed with a rubber stopper. One side of the electrode was masked in order to ensure that the Pt nanoparticles were deposited on the opposite side of the

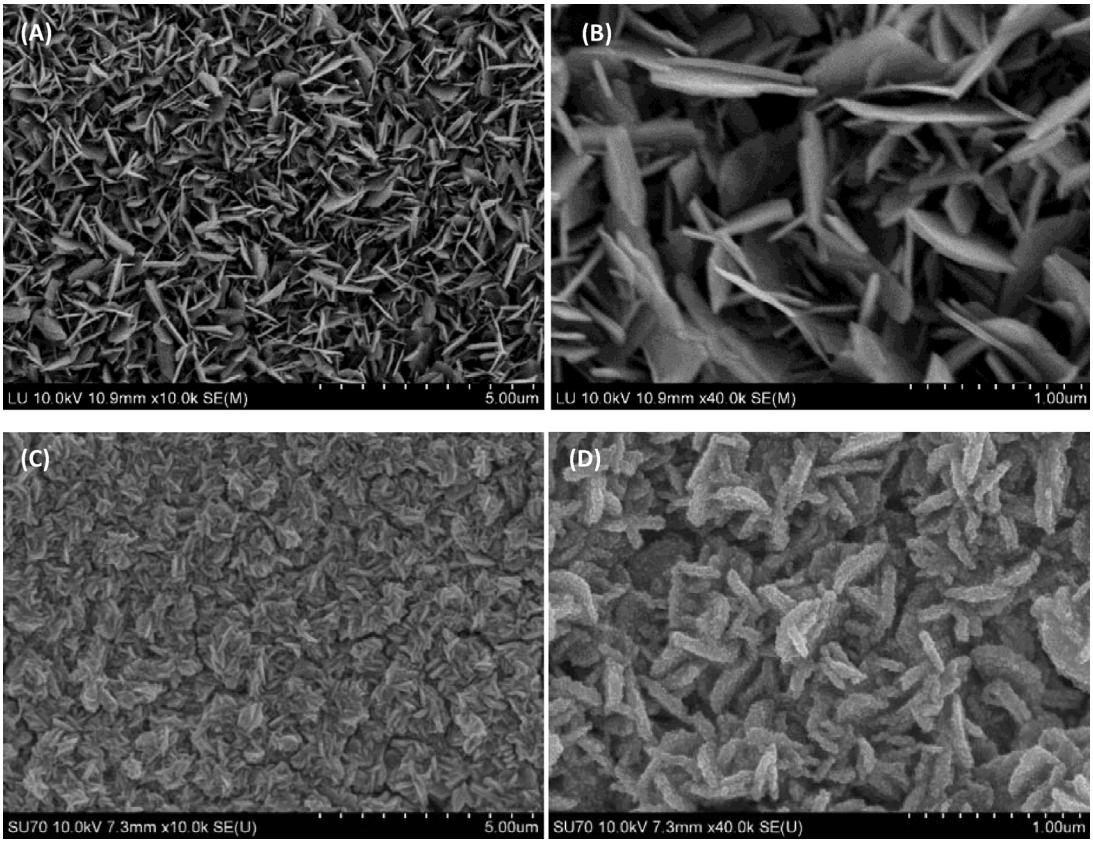

Fig. 1. SEM images of WO_3 (A and B) and WO_3–Pt (C and D).

electrode only. The electrode in the Pt solution was subsequently irradiated under UV light for one hour. The electrodes were then carefully rinsed under pure water and dried in an oven at 50 °C. The prepared bifunctional electrode was denoted as WO_3/W/WO_3–Pt, where W was the substrate; WO_3 acted as the photocatalyst; and WO_3–Pt served as the electrocatalyst.

2.4. Characterization techniques

The characterization of the crystalline phase of the synthesized samples was obtained by X-ray diffraction (Phillips PW 1050-3710 Diffractometer with Cu Kα radiation (λ = 1.5406 Å). Scanning electron microscopy (Hitachi SU 70) analysis was also performed in order to determine the surface morphology and particle size of the samples. The UV–vis absorbance spectrum was quantified using a UV–vis spectrophotometer (Varian, Cary 5E). For electrochemical characterization, a three-electrode cell system was employed. A Pt coil with a surface area of 10.0 cm^2 was used as the auxiliary electrode, whereas an Ag/AgCl electrode was employed as the reference electrode. All of the electrochemical experiments were conducted using a Voltalab PGZ301. Mott–Schottky plots were measured at a fixed frequency (500 Hz) [18]. The amplitude of the modulation potential for the electrochemical impedance measurements was 10 mV. The potential range for capacitance measurement varied from 0.0 to 2.0 V vs. Ag/AgCl.

2.5. Photocatalytic activity measurements

The photocatalytic activity of the as synthesized WO_3 was evaluated by measuring the photodegradation of RhB under visible light, with or without the applied electrode potential (1.8 V). The 25 μM RhB solution was prepared utilizing pure water (18.2 MΩ cm), which was obtained from a NANOpure® Diamond™ UV ultrapure water purification system. An Oriel system, containing a 300 W xenon arc lamp was used as the light source in this study. The lamp was allowed to warm up for 30 min prior to testing. For visible light irradiance, the source light was passed through an optical filter (Edmund Optical Co., GG420), which cut off wavelengths below 420 nm. Infrared light was removed using a water filter. Samples were collected from the reaction mixture at regular intervals, and the absorbance of the solution was measured using a UV–vis spectrometer (Varian, Cary 50). Subsequent to each reading, the solution was added back into the reaction mixture.

3. Results and discussion

With the aim of optimizing its photoelectrochemical properties, WO_3 was synthesized with different morphologies such as nanoparticles, platelets, nanorods, and nanowires, which enabled a number of unique properties that are not observed in bulk WO_3. By modifying its crystallinity, the surface energies of WO_3 may be significantly altered, which allows for the tuning of the properties of the material. Much effort has been devoted to the study of rectangular WO_3, $WO_3 \cdot H_2O$ and $WO_3 \cdot 2H_2O$ platelets, as they possess high visible light activity. To investigate the morphologies of the prepared WO_3, scanning electron microscopy was utilized, with the results shown in Fig. 1. The SEM image of the as synthesized WO_3 (Fig. 1A) revealed that platelet-like structures were formed by the hydrothermal method, and that the platelets were well distributed across the W substrate. As shown from our recent study [31], the duration of hydrothermal process had a significant effect on the thickness of the formed WO_3 platelets. When the hydrothermal vessel was heat treated for longer durations, the thickness of the WO_3 platelets increased, resulting in a significant decrease of their activity. As seen in Fig. 1B, the average length of the platelets was observed to be ~1 μm, while the width was ~50 nm. The thin

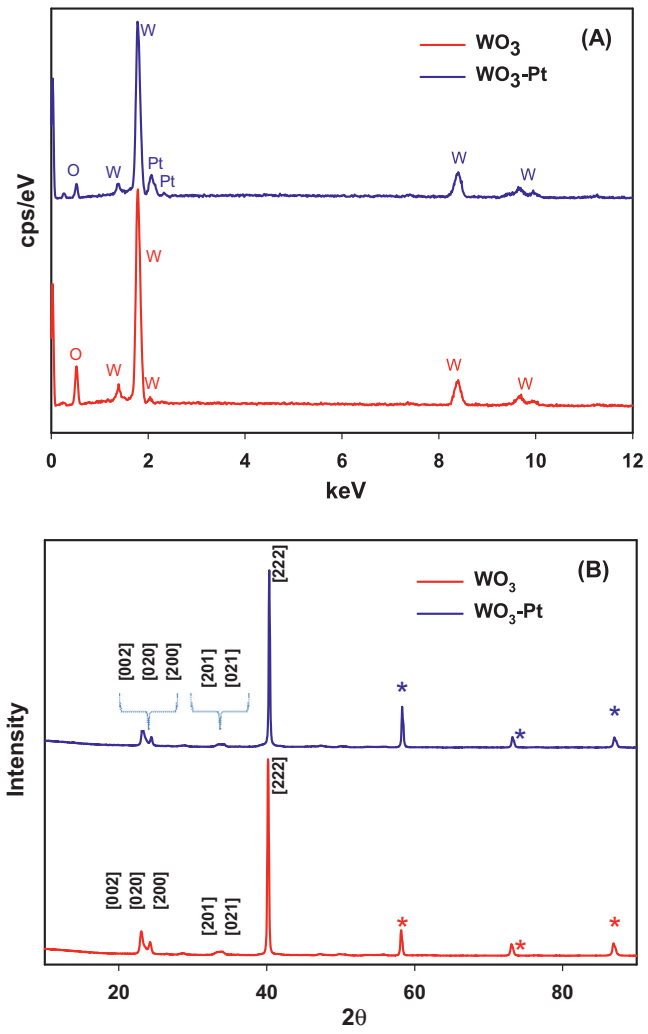

Fig. 2. Comparison of EDS and XRD results of the WO_3 (red) and WO_3–Pt (blue). The peaks marked by a star are derived from the W substrate. (For interpretation of the references to color in this figure legend, the reader is referred to the web version of this article.)

platelets resulted in an increase in the surface area of the electrodes, which made additional active sites available for reactions, thereby increasing the photocatalytic activity of the electrodes. SEM was also performed on the surface onto which Pt nanoparticles were deposited by the photochemical method, with the results shown in Fig. 1C and D. The Pt nanoparticles can be easily seen as the small dots on the WO_3 plates. It was evident that the photochemical method was very efficient for the uniform distribution of deposited Pt nanoparticles, as there were no notable Pt particle aggregates to be seen anywhere on the electrodes. These deposited Pt nanoparticles served to further increase the surface area of the electrodes.

To further investigate the composition of the WO_3 electrodes, as well as the Pt deposited WO_3, the electrodes were analyzed via EDS, with the results shown in Fig. 2A. A typical WO_3 spectrum was obtained for the WO_3 side of the electrode, as four tungsten peaks at 1.37, 1.76, 8.42 and 9.65 keV were observed. The peaks were analyzed to calculate the composition of the electrodes and a perfect 1:3 ratio for W:O was observed, confirming the formation of WO_3. For the Pt deposited side of the WO_3 electrode, the intensity of the W and O peaks was slightly less than that of the bare WO_3, as Pt covered the platelets. Aside from the W and O peaks, one strong Pt peak at 2.05, and a weak peak centered at 2.33 keV were also detected, demonstrating the presence of Pt on the surface of

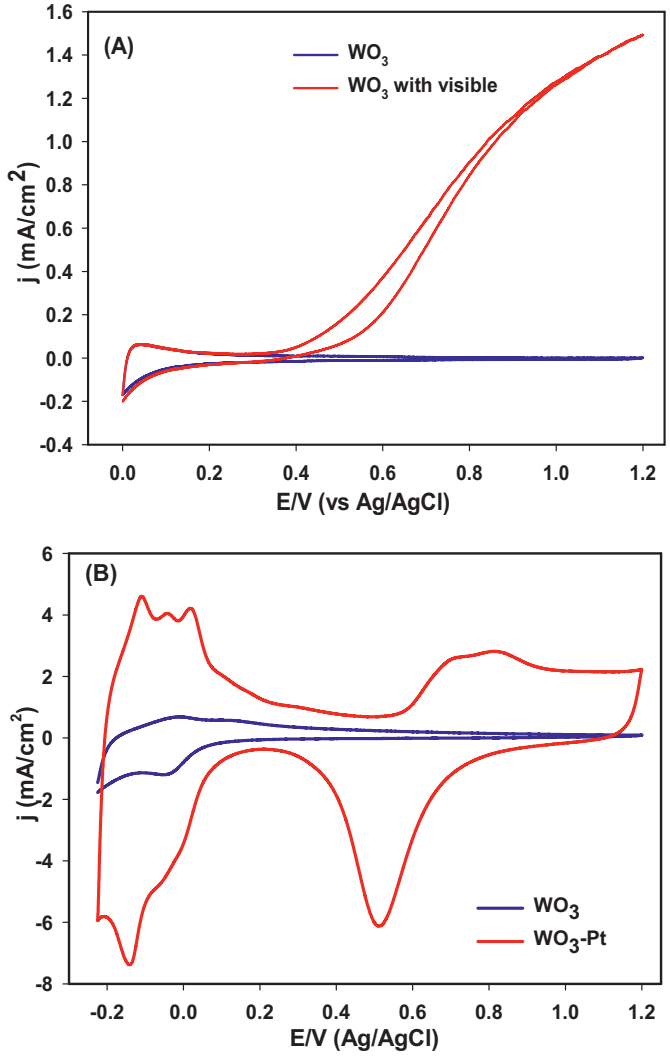

Fig. 3. (A) Cyclic voltammograms of the WO_3 electrodes under a dark condition (blue) and under visible light (red). (B) Comparison of the CVs of the WO_3 electrode prior to and following the deposition of the Pt nanoparticles. (For interpretation of the references to color in this figure legend, the reader is referred to the web version of this article.)

the electrodes, which is consistent with the SEM images shown in Fig. 1C and D.

To determine the crystalline phase, the WO_3 and WO_3–Pt samples were analyzed by XRD. Generally speaking, as seen in Fig. 2B, all of the samples demonstrated three very characteristic peaks of WO_3 at 2θ values of 23.5, 40.5, and 33.7°. According to the literature, the peak at 23.5° corresponds to the [0 0 2], [0 2 0] and [2 0 0] phases; the peak at 33.7° can be attributed to [0 2 1] and [2 0 1] planes; whereas the peak at 40.5° is due to the presence of the [2 2 2] phase. The rest of the peaks labelled by a star in the Figure are derived from the tungsten substrate. It is worth noting that even after the deposition of Pt on the WO_3 plates, no notable Pt peaks were obtained in the XRD patterns, which is most likely due to the very small volume of Pt that was deposited on the electrodes, thereby putting its presence beyond the XRD detection limits.

Cyclic voltammetry was run for the prepared samples to investigate the electrochemical behaviors of the electrodes. Fig. 3A shows the cyclic voltammograms of the WO_3 electrodes recorded in the potential range between 0.0 and 1.2 V in 0.5 M H_2SO_4 at 20 mV/s in the dark, and under the visible light irradiation. It can be seen that the electrocatalytic activity of the WO_3 electrode was low and the electrochemical current is very small in the dark. In contrast, a significant increase of the current, which was the result of an oxygen evolution reaction that occurred on the surface of the electrode, was observed under visible light irradiation, indicating that the as-synthesized WO_3 platelets had a very high visible light response. Thus, it was deemed that the fabricated WO_3 nanostructured electrodes could be effectively utilized for photocatalysis under visible light.

To characterize the electrochemical behaviors of the Pt nanoparticles, which were well-deposited on the WO_3 platelets, CV was run and compared to that of the bare WO_3 electrode, which is presented as Fig. 3B. When scanning the electrode potential from −0.225 to 1.2 V for the bare WO_3 electrode (blue curve), a small and broad peak appeared at −0.05 V, which could be attributed to hydrogen desorption. A small peak could be seen at −0.05 V in the backward scan from 1.2 to −0.225 V, due to hydrogen adsorption and hydrogenation. The red curve depicts the characteristic hydrogen adsorption and desorption peaks of Pt in the potential range of between −0.225 and +0.2 V. The distinctive hydrogen adsorption and desorption peaks may be used to estimate the electrochemical active surface area of the electrode. Assuming that the double-layer charging was constant across the entire scanned potential region, the integrated charge of the red curve, presented in Fig. 3B for hydrogen adsorption at the WO_3–supported Pt nanoparticles, was calculated to be 70.85 mC cm^{-2}, which was 308 times larger than that of a smooth polycrystalline Pt surface (0.23 mC cm^{-2}) [34]. This indicated that the Pt nanoparticles deposited on the WO_3 nanoplatelets possessed a very large electrochemical active surface area. As it is well understood that cumulative surface area plays a critical role in photocatalysis and electrocatalysis, this increase in surface area might be significant in enhancing the activity of the prepared bifunctional electrodes. Pure WO_3 electrodes have an almost non-existent level of electrochemical current, between the potential range of 0.2–1.2 V. On the other hand, Pt exhibits a high electrochemical current in the positive cycle due to the formation of Pt oxide at electrode potentials higher than 0.6 V. On the negative potential sweep, the formed Pt oxide was reduced, giving rise to a very distinct reduction peak, which was observed to be centered at 0.55 V. Several scans were performed to evaluate the stability of the deposited nanoparticles on the surface of the WO_3 electrode, and the practically overlapping CV curves showed that the prepared bifunctional electrodes were highly stable. This significant increase in electrochemical current due to the deposition of Pt may be employed as an effective electrocatalyst.

To further characterize the electronic properties of the WO_3 and WO_3–Pt coatings, Mott–Schottky measurements were carried out in a 0.1 M H_2SO_4 solution. The Mott–Schottky plot may be employed to estimate donor density (N_D):

$$\frac{1}{C^2} = \frac{2}{\epsilon\epsilon_0}\left(E - E_{fb} - \frac{kT}{e}\right)$$

where C is the capacitance of the space charge layer [$F\,m^{-2}$]; ϵ is the average value of the semiconductor dielectric constant; ϵ_0 is the permittivity of the free space charge (8.854×10^{-12} F m^{-1}); and e is the absolute value of the electron charge (1.602×10^{-19} C). The Mott–Schottky plots for the as-synthesized WO_3 and WO_3–Pt electrodes are compared in Fig. 4. For clarification, the Mott–Schottky plot for the WO_3–Pt electrode is also presented as an inset in Fig. 4. A sigmoidal plot was observed in the investigated potential range, which is typical for *n*-type semiconductors. A good linear relationship was observed between C^{-2} and the potential, in the range of between 0.0–0.40 V vs. Ag/AgCl for the WO_3 and WO_3–Pt electrodes. It is interesting to note that, following the photodeposition of the Pt nanoparticles, the donor density of the WO_3 was significantly increased. The donor densities were calculated by obtaining

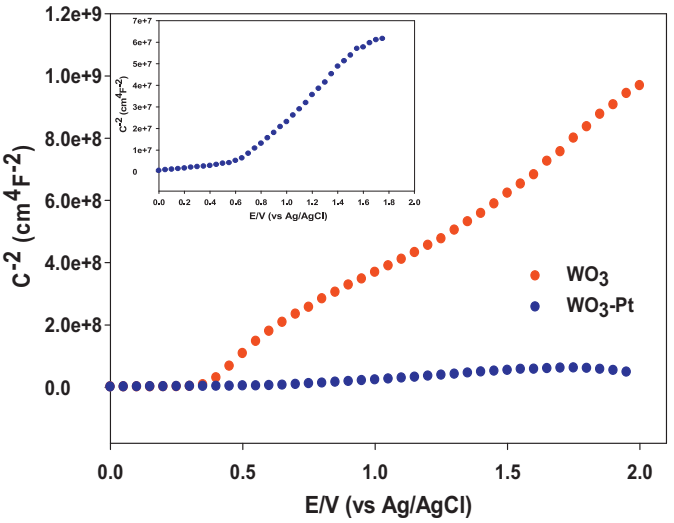

Fig. 4. Mott–Schottky plots of the WO_3 (red) and WO_3–Pt (blue) obtained in 0.1 M H_2SO_4 at 500 Hz. Mott–Schottky plot of the WO_3–Pt (inset). (For interpretation of the references to color in this figure legend, the reader is referred to the web version of this article.)

the slopes of the curves (6.0×10^{22} and 6.2×10^{23}), for the WO_3 and WO_3–Pt electrodes, respectively. This significant increase in the electron donor density of the WO_3–Pt electrodes may thus be attributed to the Pt nanoparticles that were deposited onto the WO_3 nanoplatelets, which enhanced its conductivity. This increase in electron donor density may be efficiently utilized in electrocatalysis.

To examine the photocurrent behavior of the prepared WO_3 and the bifunctional WO_3–Pt electrodes, a series of chronoamperometric measurements were performed, with the results presented in Fig. 5. A constant electrode potential of 1.8 V was applied. As shown in Fig. 5A, the as-synthesized WO_3 electrodes generated ca 1.0 mA electrochemical current in the dark. When the electrode was exposed to visible light, an approximate 0.5 mA increase in the photocurrent was observed. This elevation in the photocurrent was due primarily to an increase in oxygen evolution at the electrode surface, which was initiated by irradiation. Fig. 5B displays the results obtained when the WO_3–Pt bifunctional electrode was utilized. Interestingly, a large increase in the electrochemical current was observed as compared to the WO_3 electrode. This further validated that even a small amount of deposited Pt nanoparticles had the capacity for dramatically increasing the electrochemical current to ca. 15 times that of the bare WO_3 electrode. These results also supported the data obtained from the Mott–Schottky plots, as a ten-fold increase in the electron donor density was obtained. The bifunctional electrodes exhibited a very high electrochemical current. To examine whether the prepared electrodes might be simultaneously employed as a photocatalyst and electrocatalyst, chronoamperometric measurements were performed under visible light, with the results shown in Fig. 5C. When the electrode was exposed to visible light, an increase in the overall current was observed. This increase was approximately 3.0 mA, which was much higher in comparison to the visible light response of the bare WO_3 electrode, as seen in Fig. 5A. This conveyed that when the bifunctional electrode was employed simultaneously as a photocatalyst and electrocatalyst, there was a synergistic effect by which the overall activity of the electrode was much higher than that of the monofunctional electrode.

To further evaluate the potency of this bifunctional approach, the WO_3 and WO_3–Pt electrodes were tested for the degradation of the RhB, which is a typical organic dye pollutant, which is

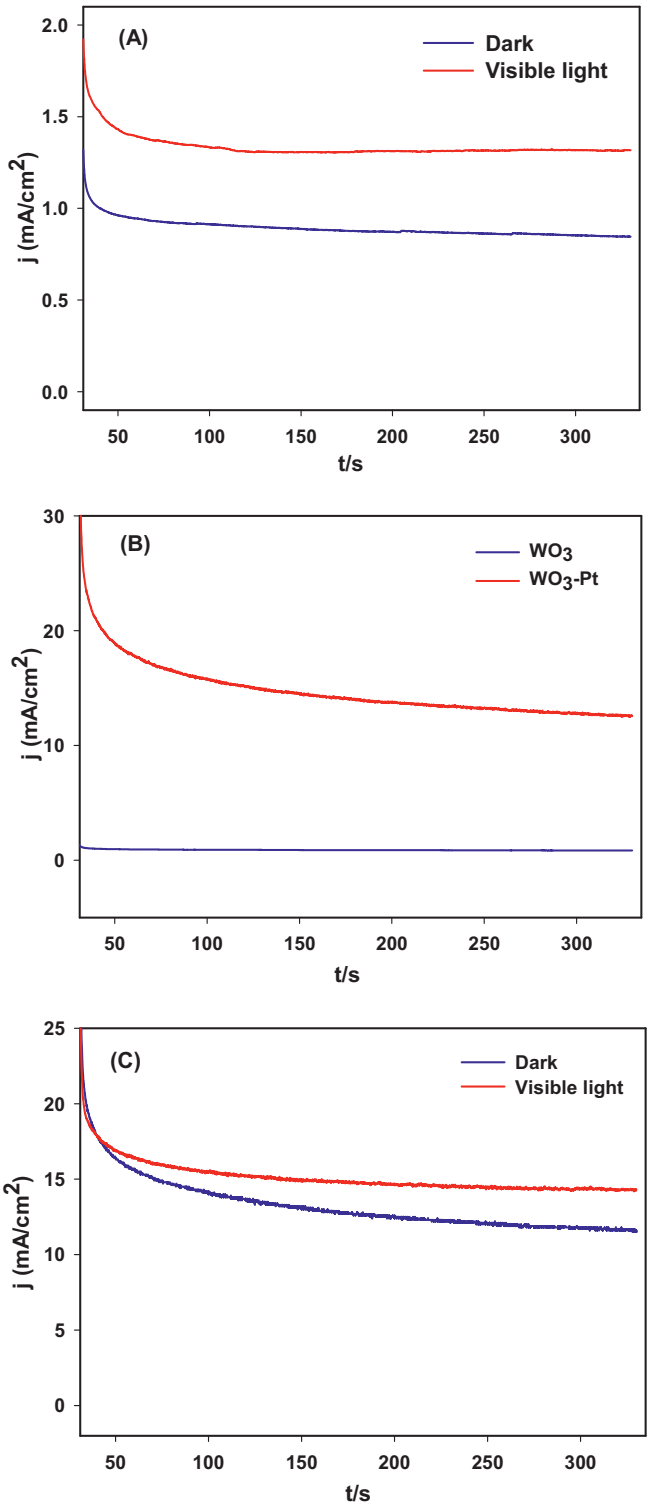

Fig. 5. Chronoamperometric curves measured at the applied potential 1.8 V of: (A) the WO_3 electrode in the dark and under visible light; (B) the WO_3 and WO_3–Pt electrodes in the dark; and (C) the WO_3–Pt in the dark and under visible light.

detrimental to aquatic ecosystems and to human populations if left untreated in ambient waterways. These degradation tests were conducted under different applied conditions. Fig. 6A presents the UV–vis absorbance spectra of the electrochemical degradation of RhB, where the WO_3 electrode was employed as an electrocatalyst under a 1.8 V applied potential. As expected, the electrochemical activity of WO_3 was quite low, and even after 70 min, the peak

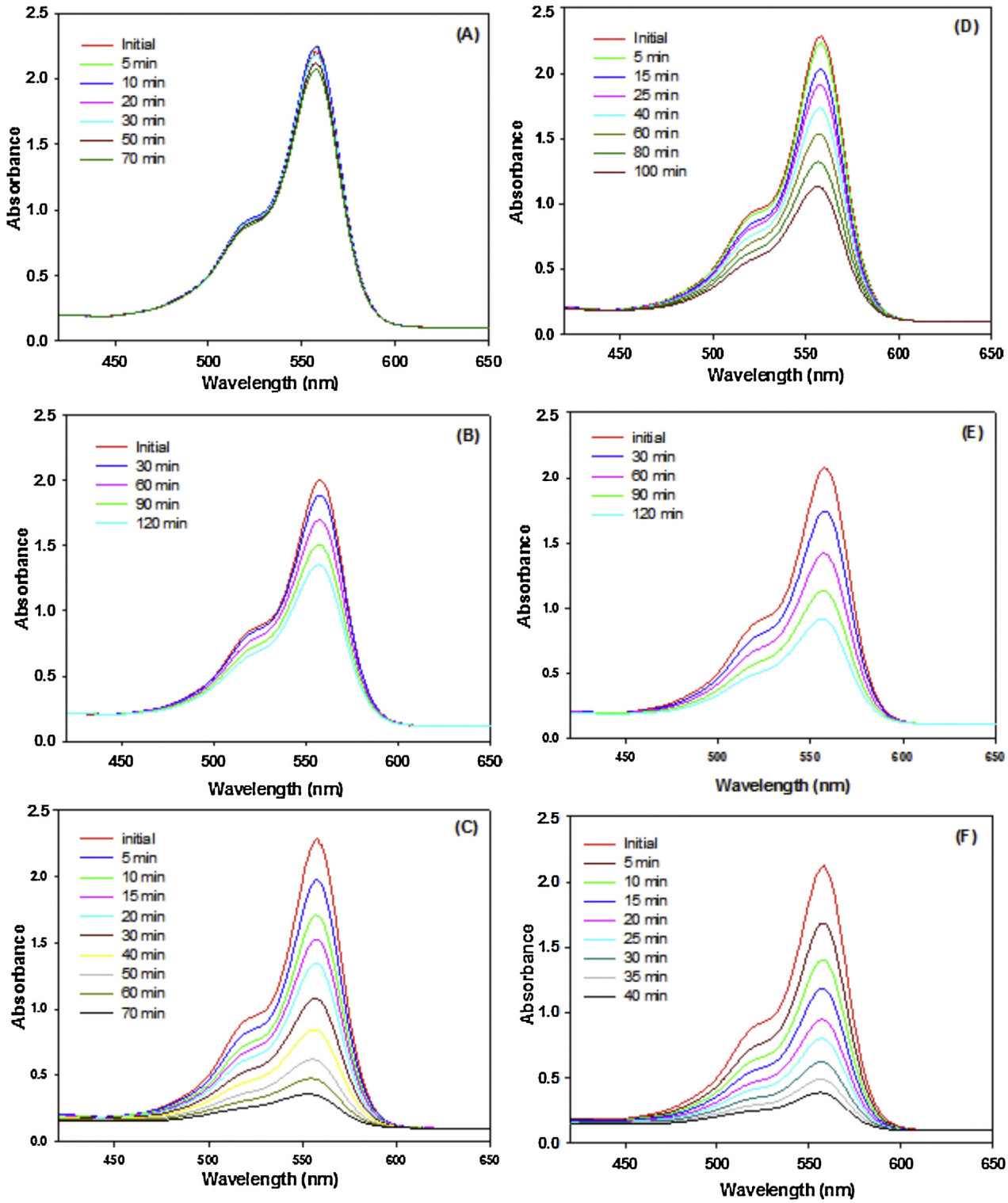

Fig. 6. The degradation curves of RhB on WO_3 under EC (A), Visible light irradiation (B) and under both EC and visible light (C). WO_3–Pt under EC (D), Visible light irradiation (E) and under both EC and visible light (F).

decreased only slightly, indicating that a very small portion of RhB had been oxidized. In contrast, the Pt deposited WO_3 electrode demonstrated a far better electrochemical activity than that of the bare WO_3 electrodes, and it can be seen from Fig. 6D that within 100 min approximately half of the RhB had been degraded.

As observed from Fig. 3A, the prepared WO_3 had a high visible light response. A series of photodegradation experiments were conducted to verify whether this highly visible light response might be translated to enhanced photocatalytic activity and the results are shown in Fig 6B. In these experiments, no external potential was applied and the WO_3 electrode was irradiated solely with visible light, demonstrating that the photocatalytic activity of WO_3 was slightly better than its electrocatalytic activity. In the presence of both applied electrode potential and visible light, the degradation

Table 1
The rate constants for the degradation of RhB calculated from Fig. 7A and B.

Sample & conditions	Rate constant (min^{-1})	R^2
WO_3 EC	1.057×10^{-3}	0.860
WO_3 Vis	3.277×10^{-3}	0.989
WO_3 EC + Vis	2.500×10^{-2}	0.998
WO_3–Pt EC	6.677×10^{-3}	0.998
WO_3–Pt Vis	6.754×10^{-3}	0.998
WO_3–Pt EC + Vis	4.190×10^{-2}	0.997

of RhB became much faster as shown in Fig. 6C, revealing that the applied potential and irradiation can impart a synergistic effect on the activity of the electrode. Interestingly, when Pt was deposited and the WO_3 electrode was utilized under the visible light, the reaction rate was two-fold in comparison to that of the bare WO_3, as can be seen in Fig. 6E. This revealed that, even though it was not activated by an applied potential, the Pt deposited on the WO_3 still contributed to the reaction via some indirect mechanism. It is most likely that the excited electrons that travelled to the surface from the conduction band were taken up by the Pt, with the effect of reducing the electron/hole recombination rate. This decrease in the recombination rate served to significantly enhance the activity of the electrode in the visible light region.

The bifunctional electrode was utilized under simultaneously applied potential and visible light irradiation to investigate whether the aforementioned high Pt nanoparticle electrochemical activity and the significant photocatalytic activity of the WO_3 might both come into play in obtaining high efficacy in the abatement of RhB, with the results shown in Fig. 6F. It can be seen that the bifunctional electrode had a much higher activity as compared to when the electrode was used exclusively for either photocatalysis or electrocatalysis. This demonstrated that there was a synergistic effect present, where both photocatalysis and electrocatalysis collaborated to convey a high catalytic response. Fig. 7A and B present the kinetic curves for the photodegradation of RhB at the WO_3 and WO_3/Pt electrode, respectively, under different conditions. The rate constant and R^2 values are listed in Table 1. R^2 values for all of the kinetic curves were close to 1, except where WO_3 was employed as an electrocatalyst. It is well known that WO_3 is a semiconductor and thus it exhibited very poor electrocatalytic activity, and due to this poor activity no linear relation was obtained. When utilizing WO_3 as an electrocatalyst, the rate constant for this reaction was calculated to be 1.05×10^{-3}, which was very low. The electrocatalytic activity of the WO_3–Pt electrode was ca. six times that of the bare WO_3 with a rate constant of 6.677×10^{-3}, showing that a very small volume (0.5 mg) of Pt nanoparticles deposited on the WO_3 nanoplatelets resulted in a considerable increase in electrocatalyic activity. WO_3 exhibited good activity under visible light, and within 120 min ~40% of the RhB was oxidized, with a reaction rate constant of 3.277×10^{-3}. The deposited Pt also enhanced the photocurrent of the electrode due to a synergetic effect by which the Pt nanoparticles most likely accepted the excited electrons, thus reducing electron/hole recombination and enhancing activity. A two-fold enhancement in the overall activity was achieved when the Pt coated WO_3 electrode was used as the bifunctional electrode.

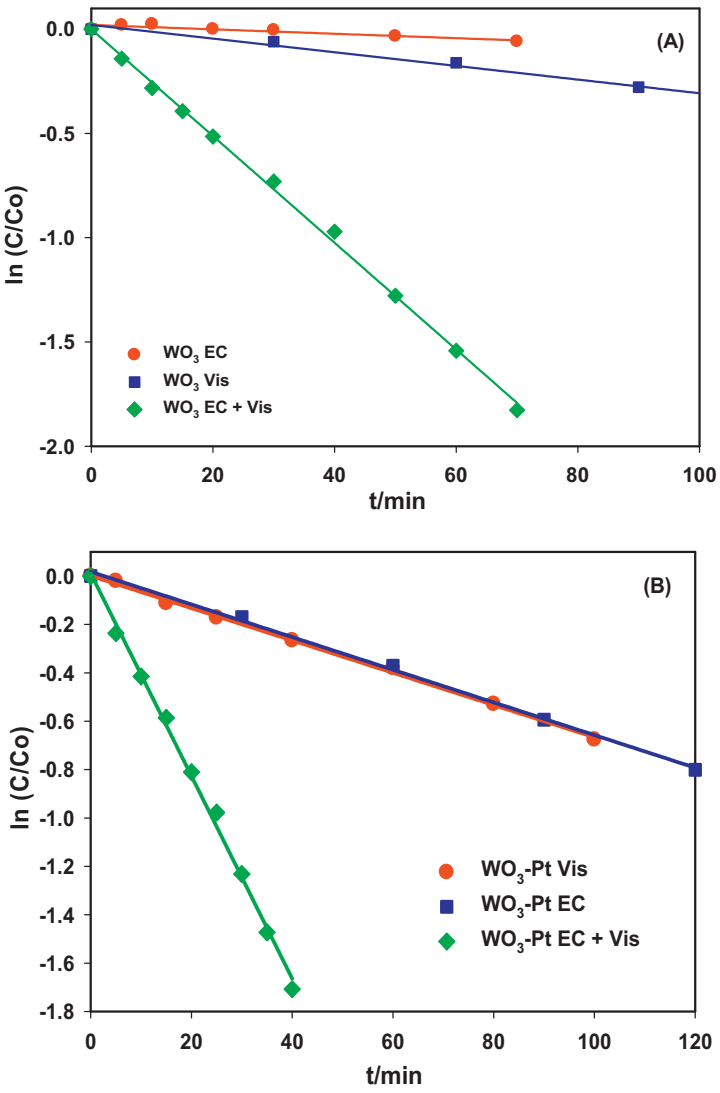

Fig. 7. Kinetic curves of the degradation of RhB on WO_3 (A) and on WO_3–Pt (B), respectively, under various applied conditions. *C* is the concentration of the RhB, and *Co* is the initial concentration.

4. Conclusions

WO_3 platelet-like structures were successfully synthesized using a facile hydrothermal method, where WO_3 nanoplatelets were directly grown onto a W substrate. The formed WO_3 nanoplatelets were well distributed across the W plate and possessed a high visible light response. The deposition of Pt nanoparticles on one side of the WO_3 electrode was achieved via a photochemical reduction method, which resulted in the uniform deposition of Pt nanoparticles on the WO_3 nanoplates. The EDS results further verified the presence of Pt on the electrodes, as well-defined Pt peaks were observed in the EDS spectrum. Cyclic voltammograms for the bifunctional electrodes indicated that the Pt nanoparticles deposited on the WO_3 nanoplatelets exhibited an extensive electrochemically active surface area, which was over 300 times higher in comparison with a smooth polycrystalline Pt surface. The RhB degradation tests on the various synthesized electrodes revealed that when the bifunctional electrodes were exposed to both visible light and applied potential, they demonstrated significantly enhanced activity. The bifunctional electrode exhibited much more robust activity as compared to when the WO_3 electrode was used exclusively as the photocatalyst, and the WO_3–Pt was used exclusively as the electrocatalyst. The new approach described in this study opens the door for the design of WO_3 based nanomaterials as high-performance photoacatalysts and electrocatalysts to address pressing environmental and energy issues.

Acknowledgements

This work was supported by a Discovery Grant from the Natural Sciences and Engineering Research Council of Canada (NSERC). A.C. acknowledges the NSERC and the Canada Foundation for Innovation (CFI) for the Canada Research Chair Award in Materials & Environmental Chemistry.

References

[1] G. Wu, S.S. Thind, J. Wen, K. Yan, A. Chen, Appl. Catal. B: Environ. 142–143 (2013) 590–597.
[2] J. Yang, Y. Zhao, C. Zhang, Y. Hu, M. Zhou, Electrochem. Commun. 34 (2013) 121–124.
[3] Y. Yavuz, A. Savas Koparal, Ü. Bakir Ögütveren, Chem. Eng. Technol. 30 (2007) 583–586.
[4] X. Qiu, Q. Zhong, M. Li, W. Bai, B. Li, Int. Biodeterior. Biodegrad. 59 (2007) 297–301.
[5] M.C. Ortega-Liébana, E. Sánchez-López, J. Hidalgo-Carrillo, A. Marinas, J.M. Marinas, F.J. Urbano, Appl. Catal. B: Environ. 127 (2012) 316–322.
[6] W. Wilson, A. Manivannan, V.R. Subramanian, Appl. Catal. A: Gen. 441–442 (2012) 1–9.
[7] P. Praus, L. Svoboda, J. Tokarský, A. Hospodková, V. Klemm, Appl. Surf. Sci. 292 (2014) 813–822.
[8] X. Fu, L.A. Clark, Q. Yang, M.A. Anderson, Environ. Sci. Technol. 30 (1996) 647–653.
[9] C. Zhan, F. Chen, J. Yang, D. Dai, X. Cao, M. Zhong, J. Hazard. Mater. 267 (2014) 88–97.
[10] J. Nilsson, A. Landa-Cánovas, S. Hansen, A. Andersson, Catal. Today 33 (1997) 97–108.
[11] S. Choi, M.-S. Lee, D.-W. Park, Appl. Phys. 14 (2014) 433–438.
[12] G. Wu, M. Tian, A. Chen, J. Photochem. Photobiol. A 233 (2012) 65–71.
[13] H. Zheng, J.Z. Ou, M.S. Strano, R.B. Kaner, A. Mitchell, K. Kalantar-zadeh, Adv. Funct. Mater. 21 (2011) 2175–2196.
[14] S.S. Thind, G. Wu, M. Tian, A. Chen, Nanotechnology 23 (2012) 475706.
[15] F. Amano, M. Tian, B. Ohtani, A. Chen, J. Solid State Electrochem. 16 (2012) 1965–1973.
[16] M. Rezapour, N. Talebian, Ceram. Int. 40 (2014) 3453–3460.
[17] X. Peng, A. Chen, Adv. Funct. Mater. 16 (2006) 1355–1362.
[18] S.S. Thind, G. Wu, A. Chen, Appl. Catal. B: Environ. 111–112 (2012) 38–45.
[19] G. Wu, J. Wang, D.F. Thomas, A. Chen, Langmuir 24 (2008) 3503–3509.
[20] S.U.M. Khan, M. Al-Shahry, W.B. Ingler, Science 297 (2002) 2243–2245.
[21] K. Song, J. Zhou, J. Bao, Y. Feng, J. Am. Ceram. Soc. 91 (2008) 1369–1371.
[22] E.A. Reyes-Garcia, Y. Sun, D. Raftery, J. Phys. Chem. C 111 (2007) 17146–17154.
[23] M. Gillet, K. Aguir, C. Lemire, E. Gillet, K. Schierbaum, Thin Solid Films 467 (2004) 239–246.
[24] S.K. Gullapalli, R.S. Vemuri, C.V. Ramana, Appl. Phys Lett. 96 (2010) 171903.
[25] Z.S. Houweling, J.W. Geus, R.E.I. Schropp, Mater. Chem. Phys. 140 (2013) 89–96.
[26] F. Amano, M. Tian, G. Wu, B. Ohtani, A. Chen, ACS Appl. Mater. Interfaces 3 (2011) 4047–4052.
[27] W.J. Li, Z.W. Fu, Appl. Surf. Sci. 256 (2010) 2447–2452.
[28] J. Rajeswari, B. Viswanathan, T.K. Varadarajan, Mater. Chem. Phys. 106 (2007) 168–174.
[29] M. Sadakane, K. Sasaki, H. Kunioku, B. Ohtani, W. Ueda, R. Abe, Chem. Commun. (2008) 6552–6554.
[30] M. Shibuya, M. Miyauchi, Adv. Mater. 21 (2009) 1373–1376.
[31] S.S. Thind, M. Tian, A. Chen, Electrochem. Commun. 43 (2014) 13–17.
[32] D. Pletcher, J. Appl. Electrochem. 14 (1984) 403–415.
[33] M. Tian, S.S. Thind, M. Simko, F. Gao, A. Chen, J. Phys. Chem. A 116 (2012) 2927–2934.
[34] M. Tian, G. Wu, A. Chen, ACS Catal. 2 (2012) 425–432.
[35] M. Shao, A. Peles, K. Shoemaker, Nano Lett. 11 (2011) 3714–3719.
[36] A. Chen, P. Holt-Hindle, Chem. Rev. 110 (2010) 3767–3804.
[37] A. Chen, Can. J. Chem. 92 (2014) 581–591.
[38] R. Abe, H. Takami, N. Murakami, B. Ohtani, J. Am. Chem. Soc. 130 (2008) 7780–7781.
[39] J. Kim, C.W. Lee, W. Choi, Environ. Sci. Technol. 44 (2010) 6849–6854.